Comparison of a new mass-concentration, chain-reaction model with the population-balance model for early- and late-stage aggregation of shattered graphene oxide nanoparticles

BABAKHANI, Peyman <http://orcid.org/0000-0002-5318-4320>, BRIDGE, Jonathan <http://orcid.org/0000-0003-3717-519X>, PHENRAT, Tanapon <http://orcid.org/0000-0003-2179-042X>, FAGERLUND, Fritjof, DOONG, Ruey-an and WHITTLE, Karl R <http://orcid.org/0000-0002-8000-0857>

Published version

BABAKHANI, Peyman, BRIDGE, Jonathan, PHENRAT, Tanapon, FAGERLUND, Fritjof, DOONG, Ruey-an and WHITTLE, Karl R (2019). Comparison of a new mass-concentration, chain-reaction model with the population-balance model for early- and late-stage aggregation of shattered graphene oxide nanoparticles. Colloids and Surfaces A: Physicochemical and Engineering Aspects, 582, p. 123862.

Comparison of a new mass-concentration, chain-reaction model with the population-balance model for early- and late-stage aggregation of shattered graphene oxide nanoparticles

Peyman Babakhani,[1,2,3*] *Jonathan Bridge,*[4] *Tanapon Phenrat,*[5,6] *Fritjof Fagerlund,*[7] *Ruey-an Doong,*[2,8] *Karl R Whittle*[2**]

[1]Earth Surface Science Institute, School of Earth and Environment, University of Leeds, Leeds LS2 9JT, UK

[2]School of Engineering, University of Liverpool, Liverpool, Merseyside L69 3GH, UK

[3]Department of Biomedical Engineering and Environmental Sciences, National Tsing Hua University, No. 101, Section 2, Kuang Fu Road, Hsinchu, 30013, Taiwan

[4]Department of the Natural and Built Environment, Sheffield Hallam University, Howard St, Sheffield S1 1WB, UK

[5]Research Unit for Integrated Natural Resources Remediation and Reclamation (IN3R), Department of Civil Engineering, Faculty of Engineering, Naresuan University, Phitsanulok, Thailand, 65000

[6]Center of Excellence for Sustainability of Health, Environment and Industry (SHE&I), Faculty of Engineering, Naresuan University, Phitsanulok, Thailand, 65000

[7]Department of Earth Sciences, Uppsala University, Villavägen 16, 75236 Uppsala, Sweden

[8]Institute of Environmental Engineering, National Chiao Tung University, No. 1001, University Road, Hsinchu, 30010, Taiwan

Submitted for publication to: *Colloids and Surfaces A: Physicochemical and Engineering*

[*]Corresponding author:

T: +44(0)7913000434, emial: p.babakhani@leeds.ac.uk

[**] Corresponding author:

T: +44(0)1517944680, emial: Karl.Whittle@liverpool.ac.uk

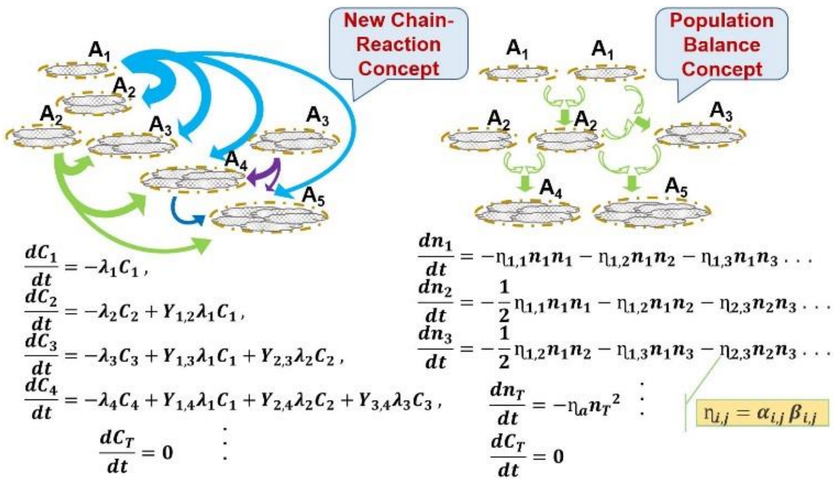

Graphical Abstract

Abstract

Aggregation as an essential mechanism impacting nanoparticle (NP) functionality, fate, and transport in the environment is currently modelled using population-balance equation (PBE) models which are computationally expensive when combined with other continuum-scale reactive transport models. We propose a new simple mass-concentration-based, chain-reaction modelling (CRM) framework to alleviate computational expenses of PBE and potentially to facilitate combination with other fate, transport, and reaction models. Model performance is compared with analytical PBE solution and a standard numerical PBE technique (fixed pivot, FP) by fitting against experimental data (i.e., hydrodynamic diameter and derived count rate of dynamic light scattering used as a representative of mass concentration) for early- and late-stage, aggregation of shattered graphene oxide (SGO) NP across a broad range of solution chemistries. In general, the CRM approach demonstrates a better match with the experimental data with a mean Nash-Sutcliffe model efficiency (NSE) coefficient of 0.345 than the FP model with a mean NSE of 0.29. Comparing model parameters (aggregation rate constant and fractal dimension) obtained from fitting CRM and FP to the experimental data, similar trends or ranges are obtained between the two approaches. Computationally, the modified CRM is an order-of-magnitude faster than the FP technique, suggesting that it can be a promising modelling framework for efficient and accurate modelling of NP aggregation. However, in the scope of this study, reaction rate coefficients of the CRM have been linked to collision frequencies based on simplified and empirical relationships which need improvement in future studies.

Keywords: Nanoparticles, environmental fate and transport, early and late aggregation, sedimentation, chain reaction model, mass concentration

1 Introduction

Production of nanomaterials is now a mainstream commercial industry. For example, graphene oxide (GO) nanosheets with 12 morphologies are routinely manufactured across 40 countries, within 15 industries, and 585 applications [1, 2]. Commercial waste streams can lead to uncontrolled spread of nanomaterials in the environment [3, 4], however, there is also a range of opportunities for the use of nanomaterials in environmental systems, e.g., environmental applications such as clean-up of radionuclide contaminated sites [5-8], agronomic applications such as the use as nano-fertilizers and nano-pesticides [9, 10], and petroleum applications such as oil/gas reservoir recovery enhancement [11, 12]. It is of paramount importance to predict and control the interactions, reactions, transport, and fate of nano-particulates in aquatic environments, a task which is already a key challenge for water and environmental engineers.

One of the critical phenomena that controls NP fate and transport as well as their reactions and functionality in environmental and engineering systems is aggregation [12-21]. Efficient integration of aggregation models with other NP fate, transport, and reaction models is crucial to enable the estimation of NP release into aquatic environments and designing NP application strategies [22-24]. Such models include: continuum models, i.e., advection-dispersion-reaction equations describing bulk mass transport over continuous spatial domains [21, 25, 26], NP life cycle assessment (LCA) which is a comprehensive modelling framework used to assess environmental and human health impacts of nanomaterials [27, 28], and abstract models including material flow analysis (MFA) or multi-media models (MMM) which are based on the mass balance principle at global and local scales [3, 29-32].

Recent investigation of the NP aggregation within systems such as porous media and surface waters revealed the need for further development of aggregation models to take realistic environmental complexity arisen from local particle resuspension into account [15]. There are several complex interactions which require consideration in a reactive transport model along with aggregation including NP reaction with existent pollutants [33, 34], interaction with background colloids and natural organic matter (hetero-aggregation), [16, 35-37], and with porous media [21, 25], as well as NP dissolution, sulfidation, and sedimentation [38-40]. Modelling approaches to aggregation with various levels of accuracy and efficiency are already available which are mostly different adaptations of PBE models [22, 40-42]. Yet a flexible, efficient, and accurate aggregation model that can be simply adapted and be coupled with other multiple-constituent models of NP fate, transport, and reaction, which are already computationally expensive, [43-45] is lacking. Furthermore, it is desirable for an aggregation model to be based on mass concentration as consistency of their main state variable with most of other models may facilitate their combination and since experimental/field data used as their input are also more readily available in terms of mass concentration [24].

In this study, we present a simple mass-concentration-based approach with the aim to model aggregation more efficiently than common PBE, with an improved or similar accuracy. A modified chain reaction model (CRM) which is based on the mass concentration, may be capable of accounting for dynamics of the aggregate populations by resembling each particle size class as a species of the reaction. We propose that such a model may be a better alternative to PBE for integration with other NP fate, transport, and reaction models due to similarity in formulation to conventional reaction equations, potential computational efficiency, and flexibility in formulation and size classification. Fundamentally, an aggregation model generally follows a second order expression if described in terms of particle number concentration [46-48]. For pure aggregation, this expression leads to a decay in the number concentration of primary particles and the total number concentration over time while the total mass concentration is constant theoretically. Likewise, a mass concentration-based model should be able to describe mass transfer among classes of the aggregates while maintaining the total mass constant. The CRM is based on a series of first-order decay expressions maintaining the total mass in the system constant. We investigate whether this approach, after being compared with analytical solution of the PBE [49, 50], can describe the change in mean particle size, PSD, and concentration of shattered graphene oxide (SGO) NP under quiescent conditions of aggregation and sedimentation across a range of solution chemistries including different electrolyte concentrations, electrolyte species, and pH. We also compare the model performance with a typical PBE, i.e., the FP technique [51] which has been widely used as a standard approach for comparison with other models [52-54]. To the best of our knowledge this is the first time that a mass-concentration CRM-based formulation is used for modelling the aggregation of colloidal particles. The previous use of the terminology 'parallel parent and daughter' in the literature of particle aggregation [55] was associated with the discretization of the PBE model.

2 Model Development

The basic CRM which has long been used in the context of dissolved contaminant transport in groundwater is as follows [56-58]:

$$\frac{dC_k}{dt} = L(C_k) - \lambda_k C_k + Y_{k-1,k}\lambda_{k-1}C_{k-1} \tag{1}$$

If $k = 1$:

$$\frac{dC_1}{dt} = L(C_1) - \lambda_1 C_1 \tag{2}$$

where C_k is mass concentration [ML^{-3}] of species k, $L(C_k)$ stands for the non-reaction terms including other transport mechanisms such as advection, dispersion, fluid sinks/sources, and/or sedimentation; λ_k is the first-order reaction coefficient [T^{-1}] for species k, and $Y_{k-1,k}$ is the yield coefficient [–] between species k-1 and k, which for physical chain-reaction models can be calculated from the stoichiometric relationship between the two species [57].

To apply this concept to aggregation mechanisms, we first assume that particle volume/size dimension discretisation is regular and sequential based on a geometric series given as $v_{i+1}/v_i = 2^{1/q}$, where q is the geometric factor and v is volume of each size class. Hence, size class k can have multiple additional primary particles compared to size class k-1. This is already a common assumption in the context of population balance modelling [40, 59, 60]. Considering the aforementioned basic CRM for such a size discretization means that when particles of size class k-1 aggregate with each other and with particles of smaller size classes, the mass concentration of their class, k-1, decays and the mass concentration of one size class larger, k, increases. Based on this concept and disregarding the term, $L(C_k)$ in Eq. (1), i.e., considering pure aggregation, one needs to assume $Y_{k-1,k} = 1$, in order to maintain the total mass of all size classes constant. This model, however, may only consider the aggregation of size class *k-1* and smaller classes resulting in creation of mass in only class k. Although due to the geometric nature of size classification, size class k can be sufficiently larger than its lower size class to accommodate aggregates produced in this way, a more accurate approach may be that aggregation of size class *k-1* and smaller classes results in redistribution of mass from class k-1 among several larger classes. Therefore, we modify the basic form of the CRM model as follows:

$$\frac{dC_k}{dt} = L(C_k) - \lambda_k C_k + \sum_{i=1}^{k-1} Y_{i,k}\lambda_i C_i \tag{3}$$

where k is the aggregate class size for which Eq. (3) is being solved. Since in the aggregation process first smaller aggregates are formed and then larger ones after collisions of the formers, the probability for transformation into larger classes should decrease with the increase in size class. We assume that $Y_{i.k}$ can be expressed as a linear function of volumes of size classes, which are already geometrically distributed, and considering total sum of $Y_{i,k}$ equal to one:

$$Y_{i.k} = \frac{v_{k_{max}-k+i+1}}{\sum_{j=i+1}^{k_{max}} v_j} \tag{4}$$

where k_{max} is the maximum number of classes considered in the model, and v is the volume of each class. For instance, assuming $k_{max}=5$ and combining both Eqs. (3) and (4) yields:

$$\frac{dC_1}{dt} = -\lambda_1 C_1 \,, \qquad k=1$$

$$\frac{dC_2}{dt} = -\lambda_2 C_2 + \frac{v_5}{v_2+v_3+v_4+v_5}\lambda_1 C_1 \,, \qquad k=2$$

$$\frac{dC_3}{dt} = -\lambda_3 C_3 + \frac{v_4}{v_2+v_3+v_4+v_5}\lambda_1 C_1 + \frac{v_5}{v_3+v_4+v_5}\lambda_2 C_2 \,, \qquad k=3$$

$$\frac{dC_4}{dt} = -\lambda_4 C_4 + \frac{v_3}{v_2+v_3+v_4+v_5}\lambda_1 C_1 + \frac{v_4}{v_3+v_4+v_5}\lambda_2 C_2 + \frac{v_5}{v_4+v_5}\lambda_3 C_3 \,, \qquad k=4$$

$$\frac{dC_5}{dt} = \frac{v_2}{v_2+v_3+v_4+v_5}\lambda_1 C_1 + \frac{v_3}{v_3+v_4+v_5}\lambda_2 C_2 + \frac{v_4}{v_4+v_5}\lambda_3 C_3 + \frac{v_5}{v_5}\lambda_4 C_4 \,, \qquad k=5$$

Since in the present study we only consider sedimentation along with aggregation, $L(C_k)$ is given as [40, 61]:

$$L(C_k) = -\frac{U_k}{Z_s} C_k \tag{5}$$

where Z_s is the sedimentation depth [L] and U_k is the sedimentation velocity of aggregates in class k [LT^{-1}] given as [62]:

$$U_k = \frac{g}{18\mu}(\rho_0 - \rho_w)(2a_0)^{3-D_f}(2a_k)^{D_f-1} \tag{6}$$

where g is the gravitational acceleration, ρ_0 is the density of primary particles, [ML^{-3}], ρ_w is the density of water [ML^{-3}], μ is the dynamic viscosity of the suspending medium

[M T^{-1} L^{-1}], a_0 is the primary particle radius [L], a_k is an aggregate radius in size class k [L], and D_f is the fractal dimension.

Reaction coefficients, λ_k, should be expressed in a way that they incorporate the nature of collision analogous to the conventional Smoluchowski model [63]. Here as a first study developing a CRM framework, we propose two different simplifying approaches to describe λ_k. For the first approach we rely on particle sizes, analogous to the so-called 'sum' collision frequency commonly used in population balance modelling [52, 64]. Such a size-based semi-empirical equation, hereafter designated as S-CRM, may be expressed as follows:

$$\lambda_k = \frac{\Lambda_S}{\tau}\left(\frac{\left|a_{k_{max}-k+1} - a_{ave,t}\right|}{a_k}\right)^{\psi}, \qquad 2 \leq k \leq k_{max} \tag{7}$$

where Λ_S is the aggregation constant of the S-CRM, mimicking the attachment efficiency in population-balance models, $a_{ave,t}$ is the equivalent radius of the geometric mean size of PSD at time t, ψ is an empirical power which depends on the size discretization approach and is assumed in the present study to be 0.5, and τ is the characteristic time [T] of aggregation (coagulation time or aggregation half-life) given as follows [46]:

$$\tau = \frac{3\mu}{4k_b T n_0} \tag{8}$$

where k_b is the Boltzman constant, μ is the viscosity of the suspending medium [M T^{-1} L^{-1}], T is temperature [K], n_0 is the initial population of particles which can be determined from the initial PSD. Equation (7) is based on this concept that the rate of aggregation, λ_k, may vary with the size of class in respect to the geometric-average size of the PSD [40]. When the geometric mean size of the aggregates grows during the aggregation process, the rates may also change for each class of particle over time. Therefore, the rates are updated in every time steps of the numerical solution. The variation of λ_k over time through $a_{ave,t}$ might help better constraining the dynamic cascading aspect of the aggregation if the model is applied in realistic environmental condition [15]. It should be noted that this model considers the Brownian motion through τ, such that increasing temperature and decreasing size can promote λ_k thereby the aggregation rate. This model may also consider the differential sedimentation mechanism of aggregation with larger differences between particles and $a_{ave,t}$ yielding larger λ_k. To clarify this, the following example is given considering a maximum number of size classes as five:

$$\lambda_2 = \frac{\Lambda_S}{\tau}\left(\frac{|a_4 - a_{ave,t}|}{a_2}\right)^{1/2} \qquad k=2$$

$$\lambda_3 = \frac{\Lambda_S}{\tau}\left(\frac{|a_3 - a_{ave,t}|}{a_3}\right)^{1/2} \qquad k=3$$

$$\lambda_4 = \frac{\Lambda_S}{\tau}\left(\frac{|a_2 - a_{ave,t}|}{a_4}\right)^{1/2} \qquad k=4$$

$$\lambda_5 = \frac{\Lambda_S}{\tau}\left(\frac{|a_1 - a_{ave,t}|}{a_5}\right)^{1/2} \qquad k=5$$

Alternatively, in the second approach to account for variations in λ_k across size classes, we directly utilize the concept of collision frequencies from the Smoluchowski model [63, 65]. However, instead of taking all possible collisions into account, we assume two types of collisions are dominant among all possible collisions. These include collisions between particles of similar size and collisions between any given particles and a particle with a geometrical mean size of PSD [66, 67]. By adding these two types of collision frequencies and nondimensionalizing each term by the maximum of their range, the following expression is resulted which is hereafter designated as C-CRM:

$$\lambda_k = \frac{\Lambda_C}{\tau}\left(\frac{\beta_{k,k}}{\beta_{1,1}} + \frac{\beta_{k,k_{ave}}}{\beta_{k_{max},k_{ave}}}\right) \tag{9}$$

where Λ_C is the aggregation constant of the C-CRM, $\beta_{k,k}$ is the collision frequency between each class of aggregates and classes of the same size; $\beta_{k,k_{ave}}$ is the collision frequency between each class of aggregates and the class that has an equivalent size with the geometric mean size of the PSD in each time step; $\beta_{1,1}$ and $\beta_{k_{max},k_{ave}}$ are the maximum of $\beta_{k,k}$ and $\beta_{k,k_{ave}}$ ranges, respectively, for all size classes. Calculations of these collision frequencies with considering all three aggregation mechanisms (i.e., Brownian, differential sedimentation, and orthokinetic aggregations) have been presented previously [40, 46] and are also available in the Supporting Information (SI). These equations are all expressed based on aggregate volumes to avoid the impact of aggregate shape on model outcomes [68]. It should be mentioned that nondimensionalizing each type of collision rate by the maximum of their range in Eq. (9) causes ignorance of the role of the two collision types in relation to each other. This may not be important in the scope of the present paper which aims to investigate whether the general formulation of CRM with simplifying assumptions about calculation of model coefficients can describe aggregation of NP.

We compared the performances of the models with an accurate population balance model solution known as the FP scheme [51] given as:

$$\frac{dn_k}{dt} = \sum_{\substack{j,i \\ v_{k-1} \le (v_j+v_i) \le v_{k+1}}}^{j \ge i} \left[1 - \frac{1}{2}\,\delta_{j,i}\right] \eta_k \alpha \beta_{j,i}\, n_j n_i - n_k \sum_{i=1}^{k_{max}} \alpha\, \beta_{k,i}\, n_i - \frac{U_k}{Z_s} n_k \tag{10}$$

where η_k is:

$$\eta_k = \begin{cases} \frac{v_{k+1}-(v_j+v_i)}{v_{k+1}-v_k}, \ v_k \leq (v_j+v_i) \leq v_{k+1} \\ \\ \frac{(v_j+v_i)-v_{k-1}}{v_k-v_{k-1}}, \ v_{k-1} \leq (v_j+v_i) \leq v_k \end{cases} \tag{11}$$

where n_k is particle number concentration of aggregates in size class k $[L^{-3}]$, v_i is the volume of solids in each aggregate in size class i, δ is Kronecker delta, and α is the attachment efficiency which is typically estimated as an aggregation constant through model fitting to experimental data. A code written in MATLAB© (Version 2016a, Mathworks, USA) was used and modified for solving this study's models, the details of which are summarised in the SI and are available in Babakhani et al. [40]. Briefly, an explicit forward Euler scheme was used for the time discretization of Eqs. (3) and (10) with an adjustable time-step. A power-law model [62, 69] was used for settling velocity and the Brinkman permeability model [40, 70, 71] was used to calculate permeability in collision frequency formulation. This model set was already found to best describe early and late stages of aggregation and sedimentation of hydroxyapatite (HAp) NP among 24 model combinations [40]. Particle size distribution observed in the beginning of each experiment was used as the initial condition in the aggregation model.

The optimization algorithm code developed in the former study [40] was also used here for calibration of parameters including aggregation constant (Λ in CRM or α in PBE) which controls the aggregation rate and fractal dimension (D_f) which controls the sedimentation velocity through Eq. (6) and collision frequencies through Eqs. (S1-S3). Adjusting both parameters was necessary to fit the model against experimental data of both early and late stages of aggregation as demonstrated in the previous study [40]. All simulation characteristics were the same for different modelling approaches. The Nash–

Sutcliffe model efficiency (NSE) coefficient [72] was used to compare different model performances against experimental data and analytical solution outputs. To calculate the mass balance, masses of particles remained suspended were integrated at the end of the simulation and was added to the integration of all mass fractions removed in each time step in a given cell at the end of simulation. The difference between this total mass and the initial mass put in the system divided by the initial mass was reported as the mass balance error. The analytical solution used for comparison with the new CRM was based on a log-normal distribution initial PSD. These are described in detail in the SI. In order to compare the CPU runtimes for different models, the models were run on a 64-bit Operating System with 3.5 GHz Intel® Xeon® CPU and 32 GB RAM.

3 Experimental

Graphene oxide (particle density 1.8 g/cm^3) was obtained from Siniocarbon, China, in powder form and dispersed in deionized (DI) water at 2 g/L. Shattered graphene oxide was then produced via intensive ultra-sonication of the GO dispersion to achieve a relatively uniform initial hydrodynamic diameter of 90 nm. This was accomplished using a probe sonication at an amplitude of 30 μm and power of 40 W for 2 h with 30-second stop following each 30-second sonication. The dispersion was then centrifuged for 30 min at 19500 $\pm$ 500 rpm to remove the fraction of larger particles. Finally, the dispersion was passed through a 0.45 μm syringe filter and the filtrate was kept in dark at 4 °C as the stock dispersion. The concentration of this dispersion was determined using gravimetric measurement and was adjusted at the set concentration (50 mg/L) before each aggregation experiment.

The evolution of aggregate size and concentration was measured over the course of each experiment at intervals of ~3.4 min using Dynamic Light Scattering (DLS) technique (Malvern Zetasizer Nano ZS, UK) as this has been used for characterizing non-spherical particles/aggregates frequently [73-75]. The valid measurement size range reported by the manufacturer is 1 nm to 10^4 nm. The same instrument was used for measuring the zeta potential. The instrument settings for size measurement were fixed for all measurements following Babakhani et al. [40]. These include using 5 runs each with a duration of 10 s for every measurement, setting the beam attenuator at a unit of 11, and the position of measurement at 6.5 mm. All experiments were conducted in duplicate for a duration >5 h. The standard deviations of the duplicate tests are reported as error bars in the final plots [76-78]. A sample volume of 3 mL was used inside the cuvette for all cases, corresponding to the measurement depth of ~2.3 cm and total water column height of ~3 cm. For fitting the model outputs we used the hydrodynamic diameter (D_H), a scattered light intensity mean also known as cumulant mean, along with the derived count rate (DCR) data used as an indicator of mass concentration [40, 79, 80]. Derived count rate was measured at different concentrations (5, 50, 500, and 1000 mg/L) of SGO to examine the correlation between the two quantities. The model fitted to D_H and DCR data was then used to describe experimental PSD obtained in the middle (150 min) and the end of each experiment (300 min). For PSD data a volume-based distribution was used, and the analysis model of the Zetasizer software was selected as "General Purpose (Normal Resolution)".

All experiments were conducted according to the following procedure: (1) prepare the particle dispersion in DI water for a final particle concentration of 50 mg/L; (2) adjust the pH at 6 ± 0.05 (or alternatively at 2.5, 4, 7.5, or 10) with NaOH/HCl (100 mM); (3) ultrasonication for 5 min, add the electrolyte (either $NaClO_4$ or $CaCl_2$), immediately vortex for 5 s, transform to a disposable cuvette, and immediately start the measurement. The whole process after taking from ultrasonicator until the start of the first measurement took 70 ± 20 s. The pH set for different cases did not show considerable variations over the course of experiment; with maximum variation for pH 7.5 decreasing to 7.1 after ~15 h.

4 Results and discussion

4.1 Comparison of the chain-reaction model with the analytical solution

Before assessing the CRM against experimental results, we first theoretically compare CRM's performance with the analytical solution of the population balance model. Since the aggregation rate constants of S-CRM and C-CRM, Λ_S and Λ_C, are not expected to scale with the attachment efficiency in the analytical solution of the Smoluchowski model which is assumed to be one, we tried to fit the modified CRMs to the analytical solution by adjusting Λ_S and Λ_C as free parameters. Over 100 min aggregation, within a fairly broad range of conditions, i.e., varying q within 1-3, D_f within 1.5-2.5, primary particle size, a_0, between 200 and 300 nm, and initial concentration, C_0, between 10 and 50 mg/L, which were totally 99 cases, the S-CRM was able to fit the total number of particles produced by the analytical solution (assuming $\alpha = 1$) very well with a mean *NSE* of 0.990±0.01 (Table S1). In a similar condition, but with a_0 range of 300 and 400 nm, and C_0 range of 1 and 10 mg/L (99 cases), the C-CRM was able to fit the analytical solution with a lower mean *NSE* 0.804±0.230 compared to that of S-CRM (Table S2). It appears that fractal dimension is the most sensitive factor in controlling the C-CRM goodness-of-fit. Using C-CRM, an increase in D_f, reduces *NSE* significantly whereas using S-CRM, an increase in D_f elevates *NSE*. The results for the aggregation rate constants for S-CRM and C-CRM fitted to analytical solution outputs are shown in Figs. S1 and S2. These results indicate that aggregation rate constants vary with factors that can affect the particle size distribution grid, i.e., q, D_f, and a_0, and parameters which can impact the collision frequency, i.e., C_0. The reason for such behaviours is not clear although they can arise from numerical difficulties at very high aggregation rates required to synchronize the numerical model with the assumption of $\alpha = 1$ in the analytical solution as well as simplifying basic assumptions of the analytical solution such as collision frequency being described only by Brownian collisions. Overall, these results suggest that the modified CRM is able to describe the aggregation phenomenon in most of cases when compared to a simplified analytical solution.

4.2 Experimental results

The results of hydrodynamic size evolution and DCR are presented in Figs. 1 and 2. The late stage of aggregation/sedimentation, i.e., where the slope of size versus time changes significantly, does not appear within 5 h for electrolyte concentrations ≤0.5 mM $CaCl_2$ and ≤20 mM $NaClO_4$ at pH 6 (reaction limited regime, RLA) whereas above these thresholds the late stage appears as a significant reduction in the slope of the D_H curve versus time. Likewise, at pH <6 and 20 mM $NaClO_4$, the late stage of aggregation appears in D_H curves. These are in general agreement with aggregation trends of hydroxyapatite (HAp) NP observed in the previous study [40]. It appears that critical coagulation concentration (CCC) [81] above which the system is considered under the diffusion limited regime (DLA), is between 0.5-1 mM for $CaCl_2$ and between 30-50 mM for $NaClO_4$. Considering matched D_H curves for SGO size evolution at 0.5 $CaCl_2$ and 30 mM $NaClO_4$, CCC ration of monovalent to divalent electrolyte is estimated to be in the range of 50–60 which is within the range calculated by Schulze-Hardy rule, i.e., 4–64 [81] and in agreement with ratios measured for GO elsewhere [82]. Considering the proportionality of CCC with $\zeta^4 z^{-2}$ (where ζ is zeta potential and z is valence of the electrolyte) one can also calculate the CCC ration of monovalent to divalent electrolyte

[83, 84]. According to the zeta potential data, given in Fig. S3, ζ ranges from -25.7 to -19.9 mV for monovalent and from -17.6 to -7.2 for divalent electrolytes at their corresponding CCC ranges assumed above. This yields CCC ration of monovalent to divalent electrolyte from 5.9 to 20.3 which is still within the boundaries of the Schulze-Hardy rule but lower than the ranges calculated above. There is an ongoing research to understand such discrepancies [83-86].

At moderate concentration of $CaCl_2$ (0.5 mM), DCR/DCR_0 demonstrates significant increase over time whereas at 30 mM $NaClO_4$, DCR/DCR_0 tends to show a mild decreasing trend (Fig. 1d,e). The increase in DCR/DCR_0 is similar to the previous observations of Babakhani et al. [40], for HAp NP in presence of 0.3 mM $CaCl_2$ at pH 6 (RLA regime). Nevertheless, this behaviour seems to be specific to the presence of $CaCl_2$ since this is not noticeable at 30 mM $NaClO_4$ although a slight rise in DCR/DCR_0 is observed for lower $NaClO_4$ concentrations—5 and 10 mM (Fig. 1d,e). While in a high-rate aggregating system variation in DCR/DCR_0 may represent the variation in the normalized concentration (C/C_0) of NP, at a low-rate aggregating system DCR/DCR_0 may not be a proper indicator of NP C/C_0. This is because in this regime the sedimentation is not significant and C/C_0 is expected to be constant while DCR/DCR_0, especially in presence of $CaCl_2$, demonstrates an increase above unity which might be an impact of scattered light being dependent on particle size, and appearing only when the change in concentration due to sedimentation is not significant. It should be noted that the use of DCR/DCR_0 as a representative of mass concentration in high-rate aggregation systems or DLA conditions was verified in the previous study [40] by being described with a size-matched model. Additionally, when there is no aggregation in the system SGO used in the present study shows a linear correlation between mass concentration and DCR data with a goodness-of-fit coefficient r^2 =0.952 and P value $\gg$ 0.05 with the null hypothesis being significant difference if $P < 0.05$ (Fig. S4, Supporting Information). Nevertheless, the dependency of the scattered light intensity on the particle size is theoretically proportional to the third power, in contrast to its dependency on mass concentration which is linear [87]. Thus, in an aggregating system in which the size grows over time, DCR's proportionality to mass concentration may not necessarily follow a linear trend. Overall, the reason for the rise of DCR/DCR_0 above unity in a slow-aggregation regime under some solution chemistries is not clear in the scope of the present study, and the real proportionality of DCR on mass concentration in an aggregating system is also not clear currently. These may be addressed in future studies.

4.3 Model fit results

Nash–Sutcliffe model efficiencies for different model fits to D_H data are shown in Table 1 and modelled curves versus observations of D_H and DCR are illustrated in Figs. 1 and 2. On average, FP, S-CRM, and C-CRM, show close mean NSE to D_H curves with, 0.29, 0.33, and 0.36, respectively. The reason for low overall mean *NSE* values is that in cases where observation data are close to their mean, i.e., at low aggregation rates such as cases at low electrolyte concentrations of 0.1 mM $CaCl_2$ and 5 mM $NaClO_4$ or at high pH of 10, even though visually a good match is obtained between the two graphs of the observation and modeled data, *NSE* is not reaching a value close to one as expected, and instead show values close to zero.

Based on visual assessment of the fittings, the performance of S-CRM method is slightly poorer than other methods in terms of reproducing the sudden change in D_H gradient between early and late stages of aggregation under the DLA regime (1 mM $CaCl_2$ and 50 mM $NaClO_4$, Fig. 1b,c). It seems S-CRM and FP are less capable of mimicking the straight log linear curve of D_H under the RLA regime (0.5 mM $CaCl_2$ and 30 mM

$NaClO_4$) than C-CRM method which also reproduces well the change of D_H slope under the DLA regime. This is consistent with the maximum mean *NSE* obtained for the C-CRM.

Considering the DCR data (Figs. 1d,e,f and Fig. 2b), none of models reproduces the rising behaviour of DCR curves at intermediate IS because the simple explicit decay sedimentation term employed in this study is not expected to reproduce increase in the concentration. It should be noted that such a sedimentation model, which does not involve a partial derivative in respect to depth, is simple and does not require spatial discretization in the numerical solution thereby bypassing some of numerical issues/restrictions. However, it is still not clear to what extent the depth profiles resulted from this model match the reality, which is a subject of future studies. Within the DLA regime, all models can, to some extent, reproduce the nonlinear reduction in normalized DCR. In describing DCR trends within this regime, FP technique appeared to perform best followed by S-CRM and C-CRM (Fig. 1d,e,f and Fig. 2b).

Model-produced PSDs based on D_H and DCR-matched models are shown in Figs. 3 and S5. It appears that none of the models can reproduce the PSD in all cases. In most of the cases, both modified CRM approaches tend to preserve the initial position of the PSD over time, although the heights of the peaks are changing. This is more noticeable for the C-CRM than S-CRM. The fixed pivot approach exhibiting considerable movement of the PSD position, appears to overestimate the experimental PSD, and cannot reproduce the stationary stage of the PSD, especially toward the late stage of aggregation. It is possible that in the case of CRM the mass gradually moves to larges size classes and becomes subject to sedimentation before it appears as movement of the PSD. Such a steady-state or equilibrium condition of the PSD has frequently been used as a basic assumption in model developments [24, 88-90]. Although FP overtimes the position of PSD, it can reproduce the overall shape of the observed PSD generally better than other methods. On average, in terms of reproducing both shape and position of PSD, the size-based CRM performs relatively better than the other two methods because it produces PSDs with closer positions to observed PSDs, than that produced by FP and with a closer shape to observed PSD than that resulted by C-CRM (Figs. 3 and S5). It should be noted that particle size measurement using DLS for polydisperse samples has been criticized for being affected by the larger size fraction of the size spectrum, because the scattered light intensity is proportional to the size by a power of six [87]. Such uncertainties in the measurement approach makes it complex to find a model which reproduces all aspects of PSD.

4.4 Estimated parameter trends

The trends of estimated parameters including aggregation rate constants (Λ_S, Λ_C, or α) and fractal dimension, D_f, are shown in Fig. 4 for different solution chemistries. According to this figure, the trends of aggregation rate constants are consistent among all cases. Unlike HAp NPs in a previous study [40], which exhibited multimodal trends of α estimated using the FP method with IS, here FP-estimated values of α for SGO show a positive log linear trend with IS with r^2=0.93 and 0.97 for $NaClO_4$ and $CaCl_2$, respectively (Fig. 4a,b) and a negative semi-log linear trend with pH with r^2 = 0.98 (Fig. 4c). Interestingly, consistent with the trends of α, the CRM-estimated aggregation constants Λ_S and Λ_C display a positive log linear trend with IS (r^2=0.84 for C-CRM and r^2=0.85 for S-CRM in $NaClO_4$ solution and r^2=1.00 for both C-CRM and S-CRM in $CaCl_2$ solution) and a negative semi-log linear trend with pH (r^2=0.73 for C-CRM and r^2=0.86 for S-CRM). The gradients of the lines fitted to Λ_S and Λ_C versus IS and pH match very well with that of α (P=0.55 and 0.61 $\gg$ 0.05) (Fig. 4a-c).

Fractal dimension generally increases with IS (Fig. 4d,e) and decreases with pH (Fig. 4f), which is in agreement with Chowdhury et al. [91] measuring D_f for TiO_2 NP using static light scattering (SLS). Yet unlike aggregation constant patterns, D_f trends are not effectively linear (Fig. 4d-f). This is mostly because of large D_f values determined at lowest IS which emanates from the fact that at the lowest IS, the aggregation is not operative and therefore particles remain in their primary size which should have a geometry close to Euclidian thereby having a D_f close to 3 [40]. Estimated D_f in the present study yields close ranges for the three models, namely, from 1.50 to 2.86 for the FP model, from 1.48 to 2.80 for C-CRM, and from 1.70 to 2.70 for S-CRM. Large values of D_f (2.27-2.8) were commonly determined at high IS (DLA regime) while low D_f values (1.48-1.99) were estimated at intermediate IS (RLA regime). Although similar ranges for D_f under DLA have frequently been reported [62, 92], this is opposite to common ranges of D_f, reported for aggregates formed in controlled condition where they are not subject to restructuring, i.e., D_f close to 2.2 within RLA regime and close to 1.7 within the DLA regime [46, 71, 91, 93]. The underlying reason for D_f values differing from common ranges is attributed to restructuring of aggregates at greater depths during the late stage of aggregation in quiescent condition [40] as the typical trends and ranges of D_f were achieved when the FP model was fitted only to the early stage of aggregation, or when the measurement depth was reduced to just below the surface of the water column.

Overall, the general consistency of parameter trends suggests that CRM model parameters although do not scale with those of FP approach, generally show similar trends with FP parameters in respect to physical factors such as electrolyte concentration and pH. Aggregation rate parameters can be considered variable with size in order to include the impact of solution chemistry such as zeta potential and ionic strength through the DLVO theory in a forward prediction mode similar to the previous study [40]. This is beyond the scope of the present study which aims to test the ability of CRM in 'describing', rather than 'predicting', the aggregation behavior of NP.

4.5 Comparison of model efficiency and accuracy

The results of model run time and mass balance error for every case simulating an experimental duration of 18000 s are reported in Table 2. The computational times vary widely among experimental cases due to different aggregation rates, initial PSDs, etc. The mean runtime for the FP technique is 6.14 min. While it is complicated to compare runtimes across different studies due to differences in computer systems, software versions, number of grid points, simulation duration, initial conditions, etc., considering the simulation duration in the present study (18000 s), it appears that these runtimes for the FP method are comparable with elsewhere [22, 53, 54].

Interestingly, the modified CRMs turn out to be about one order-of-magnitude faster than the FP method with mean runtimes 0.92±1.15 min for C-CRM and 0.49±0.53 min, for S-CRM. The FP technique is a widely-accepted population-balance model [53, 94], with an ability to preserve the two properties, population and mass. The MATLAB code for solving this model was already verified against analytical solutions of the population balance given for different initial conditions [40]. Here the FP method which is inherently a PBM yields a fairly low average absolute mass balance error (3.9×10^{-2} %). However, the proposed models of the present study which are inherently mass-balance models show even lower absolute mass balance errors; 4.2×10^{-6} % and 1.1×10^{-5} %, for C-CRM and S-CRM models, respectively, suggesting that the use of mass balance in modelling aggregation not only leads to a more efficient simulation but also enhances the accuracy.

It should be noted that based on the current formulation of CRM models, the outcomes might be dependent on the particle size grid configuration such as the maximum number of size classes. A maximum number of 100 size classes may be recommended as a standard that is sufficient to capture PSD evolutions in the environmental systems, and thus this can be fixed as part of the model. We further investigated the influence of the number of size classes on model results. The outcomes presented in Figs. S6 and S7, revealed that at high aggregation rates the dependency on the number of bins is not significant for both C-CRM and S-CRM while at low aggregation rates this dependency is considerable. Further, we fitted the S-CRM model to the analytical solution results of the Smoluchowski model. As shown in Fig. S8, this investigation revealed that there is a log linear relationship between the adjusted S-CRM rate constant and the number of size classes in all cases, suggesting that the impact of number of size classes may be offset from aggregation rate constants in future studies. As already mentioned in Section 4.1 the impact of variation in particle size grid configuration causing changes in the aggregation constant fitted to the analytical solution might also arise from simplifying assumptions of the analytical solution and possible numerical inaccuracies of any given numerical approaches in certain configurations of the particle size grid [40, 53]. Such factors can deviate the trends of aggregation constants of numerical models from that of analytical approach whereas consistent trends are obtained across different numerical methods.

5 Conclusions

In this study we propose a new modelling framework based on a mass-balance chain reaction formulation. This includes a series of first-order, coupled decay reaction expressions with mass concentration as the main variable. Two simplifying approaches based on size (S-CRM) or collision frequencies (C-CRM) were proposed for considering variations in the decay-reaction rates in terms of aggregate size classes. The two CRM approaches both can generally fit well to analytical solutions of the aggregation model with a log normal initial PSD within a range of conditions. When fitting to a range of experimental data for early and late aggregation and sedimentation of SGO, the performances of both approaches were generally similar to or better than that of the FP model which is a standard PBE. The new modelling framework was found on average one order-of-magnitude faster than the FP method while yielding a lower average mass balance error. In contrast to FP, modified CRM approaches tended to show a steady-state or equilibrium condition for the shape of the PSD at moderate or low aggregation rates. Similar trends for aggregation rate constants, estimated from model fitting to experimental data, were obtained for all models, and close ranges were obtained for fractal dimensions, suggesting that model parameters for the proposed modified CRM are meaningful and may follow conventional models. Although future studies may present more accurate relationships for CRM reaction rate and yield coefficients, the use of two simplifying/empirical preliminary approaches in this study for reaction rates demonstrated generally similar performances suggesting that the model is not much sensitive to these coefficients and therefore the simplifying assumptions taken in developing current relationships may not affect the model outcomes significantly.

While there are uncertainties in the experimental results, parameter calibration process, and the basic assumptions of model relationships, based on the overall agreement between the modified CRM and analytical/numerical solutions of PBE as well as experimental data of SGO aggregation we conclude that a CRM formulation is able to describe NP aggregation phenomenon. Owing to its flexibility in formulation, low computational expenses, and the use of mass concentration, the CRM may also offer potentials for modelling aggregate breakage, e.g., using negative rate coefficients [24], and may be a suitable option to be modified for modelling hetero-aggregation of NP with background colloids as well as the adsorption of other solute contaminants. The CRM can be a useful approach not only for modelling the aggregation of engineered NP in environmental media, but also for modelling the aggregation of particulate species in other contexts such as biogeochemistry where the complex network of the reactions in the reactive transport model makes incorporation of population balance models computationally cumbersome if possible at all. Overall, this study demonstrates that a chain-reaction model widely used for describing chemical and nuclear reactions can be used for modelling aggregation of colloidal particle.

Acknowledgements

Support to PB from the University of Liverpool and National Tsing Hua University is gratefully acknowledged. This work was partly funded by the Taiwan's Ministry of Science and Technology (MOST) under the grant No. 104-2221-E-009-020-MY3. Sheffield Hallam University provided research support time for JB. We gratefully acknowledge Chien-Hou Wu and Chung-Yi Wu (National Tsing Hua University) for providing full-time access to the DLS instrument and Ming Li (University of Liverpool) for fruitful discussions on the modelling. We also thank anonymous reviewers for their constructive suggestions which helped us to improve the paper.

Figure Captions.

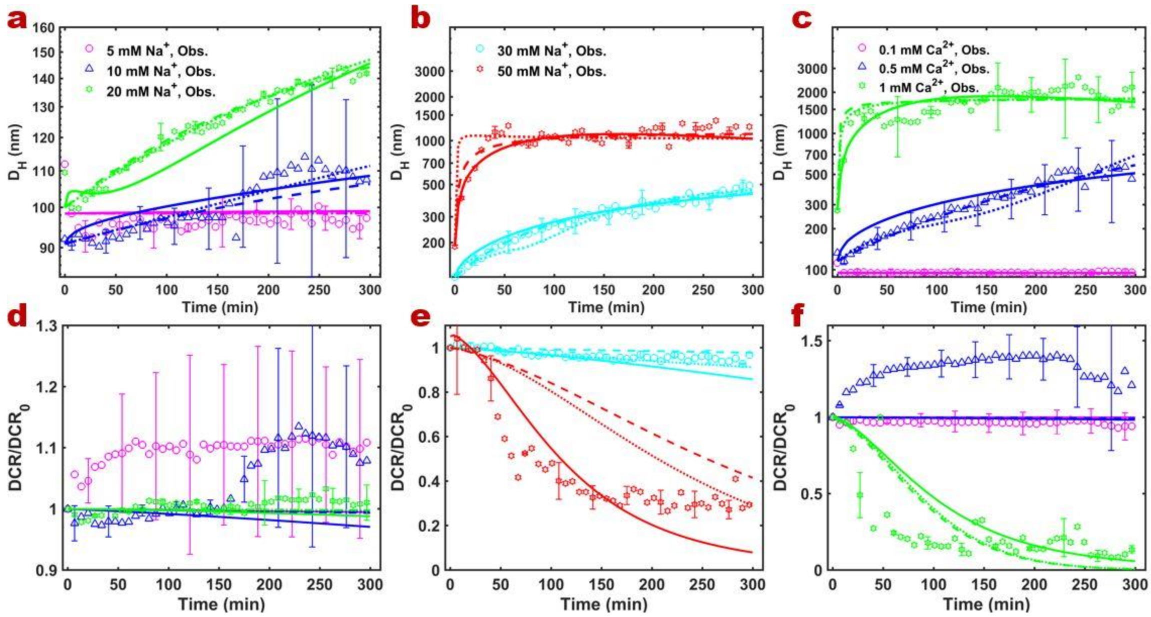

Figure 1. Evolutions of size (a-c) and change in normalized derived count rate (DCR/DCR_0), (d-f) for SGO NPs in electrolyte species $NaClO_4$ (a,b,d,e) and $CaCl_2$ (c,f) with a fixed pH at 6. Continuous lines represent FP, dash lines represent C-CRM technique, and dot lines represent the S-CRM model outcomes.

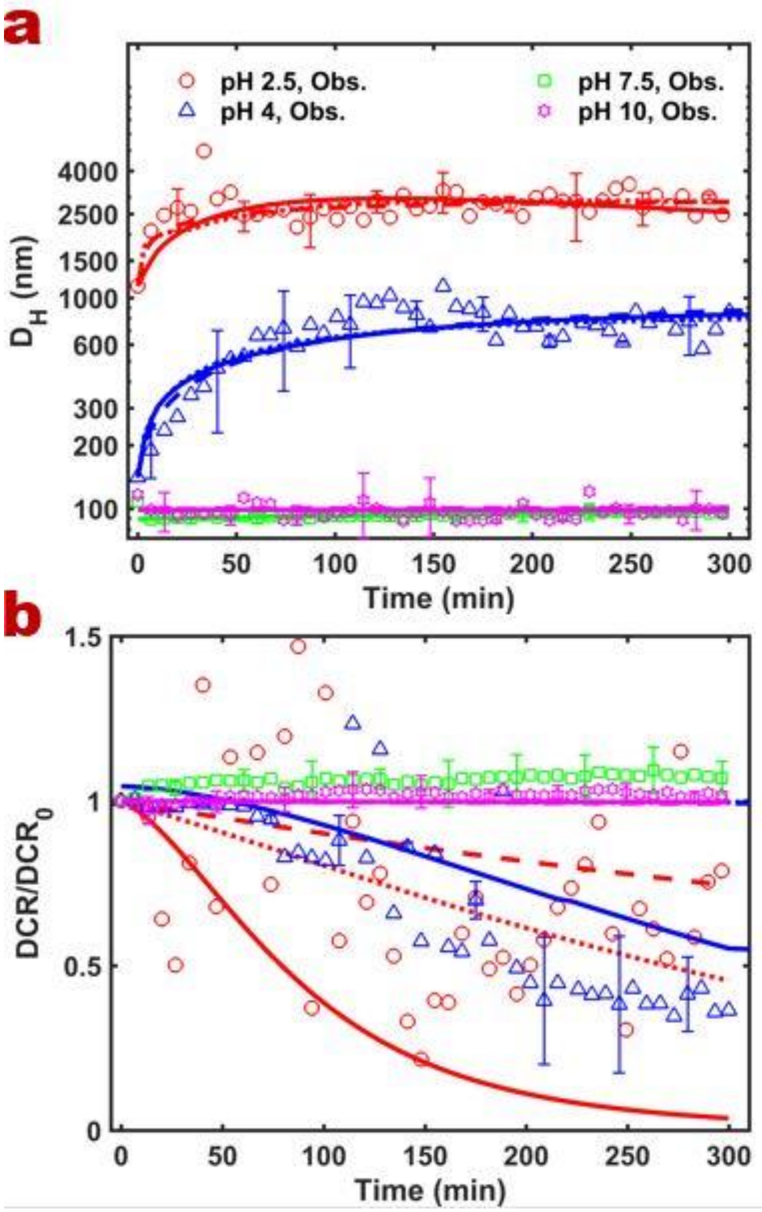

Figure 2. Evolutions of Size (a) and change in normalized derived count rate (DCR/DCR_0), (b) for SGO NPs at various pH with a fixed IS at 20 mM $NaClO_4$. Continuous lines represent FP; dash lines represent C-CRM technique, and dot lines represent the S-CRM model outcomes.

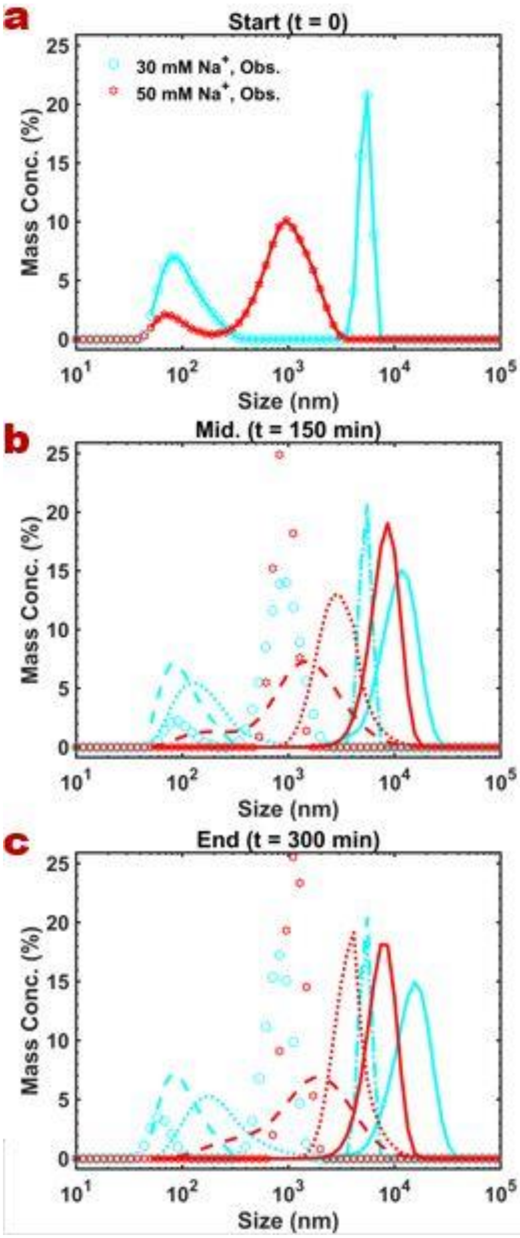

Figure 3. Comparisons of PSD for SGO NPs at 30 and 50 mM $NaClO_4$ with a fixed pH at 6 and at the middle (t=150 min, b) and the end of experiments (t=300 min, c). Continuous lines represent FP; dash lines represent C-CRM technique, and dot lines represent the S-CRM model outcomes. It should be noted that lines in panel (a) only show the initial condition of the model.

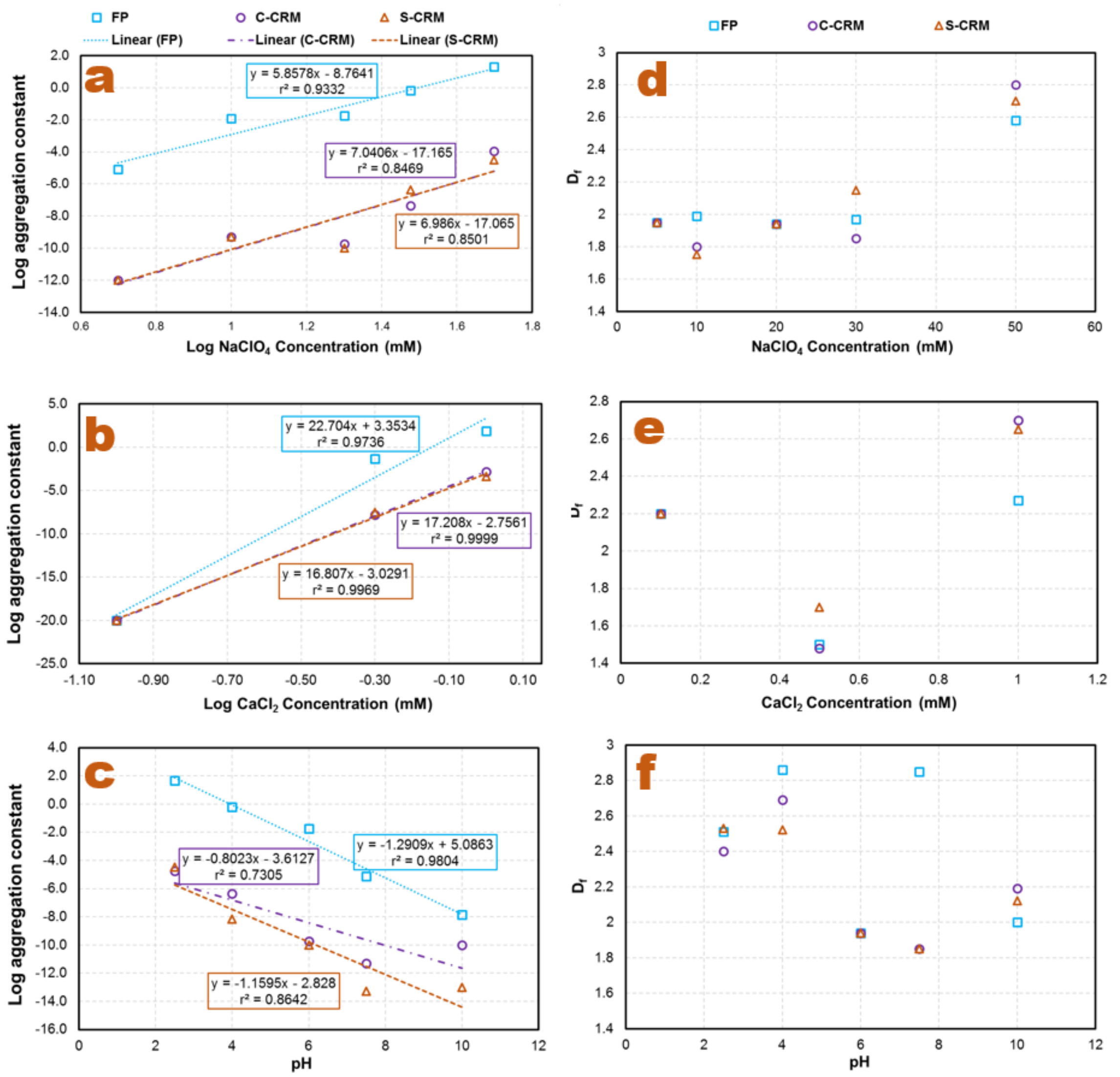

Figure 4. Estimated parameter trends for different models: aggregation rate constants (α, Λ_S, and Λ_C for FP, S-CRM, and C-CRM approaches), vs electrolyte concentration (a,b), and vs pH (c), and fractal dimension, D_f, vs electrolyte concentration (d,e) and vs pH (f).

Table 1. Nash-Sutcliff determination coefficient, NSE, for fittings to hydrodynamic diameter data with different models across various solution chemistries.

pH	**Electrolyte concentration**	**FP**	**C-CRM**	**S-CRM**
6	0.1 mM $CaCl_2$	-0.093	-0.092	-0.092
	0.5 mM $CaCl_2$	0.862	0.947	0.830
	1 mM $CaCl_2$	0.505	0.340	0.422
	5 mM $NaClO_4$	-1.141	-0.826	-0.843
	10 mM $NaClO_4$	0.683	0.694	0.842
	20 mM $NaClO_4$	0.827	0.978	0.971
	30 mM $NaClO_4$	0.923	0.940	0.912
	50 mM $NaClO_4$	0.447	0.587	0.178
2.5	20 mM $NaClO_4$	-0.245	0.067	-0.072
4		0.492	0.488	0.537
7.5		0.257	0.256	0.255
10		0.000	-0.033	0.000

Table 2. Comparison of the model run times and mass balance errors in a single-run mode based on parameters estimated from the calibration process.

pH	Electrolyte concentration	Model Run Time (min)	Mass balance error (%)	Model Run Time (min)	Mass balance error (%)	Model Run Time (min)	Mass balance error (%)
		FP		**C-CRM**		**S-CRM**	
6	0.1 mM $CaCl_2$	3.77	-7.1E-14	0.06	-2.8E-14	0.04	-2.8E-14
	0.5 mM $CaCl_2$	0.60	-2.1E-04	0.28	5.3E-10	0.04	9.4E-11
	1 mM $CaCl_2$	1.23	-4.1E-01	2.22	-9.5E-06	1.48	-9.1E-05
	5 mM $NaClO_4$	30.06	1.1E-08	0.13	-2.8E-14	0.09	1.4E-14
	10 mM $NaClO_4$	0.94	-2.9E-05	0.29	-1.0E-08	0.20	-1.5E-08
	20 mM $NaClO_4$	5.99	-3.8E-05	0.66	2.1E-11	0.47	8.4E-13
	30 mM $NaClO_4$	1.32	-2.4E-05	0.27	-4.7E-06	0.18	-5.0E-06
	50 mM $NaClO_4$	4.73	-5.1E-02	2.08	-3.6E-05	1.34	-3.8E-05
2.5	20 mM $NaClO_4$	2.59	4.4E-07	1.03	1.9E-08	0.70	2.5E-09
4		18.17	-3.9E-07	3.67	1.1E-13	1.10	2.8E-14
7.5		0.46	3.1E-12	0.07	-2.7E-08	0.05	-1.0E-08
10		3.87	4.0E-12	0.22	3.0E-13	0.12	-1.4E-14

References

[1] A. Zurutuza, C. Marinelli, Challenges and opportunities in graphene commercialization, Nature nanotechnology, 9 (2014) 730.

[2] Nanotechnology-Products-Database, http://product.statnano.com/search?keyword=graphene+oxide, 2018.

[3] A.A. Keller, S. McFerran, A. Lazareva, S. Suh, Global life cycle releases of engineered nanomaterials, J. Nanopart. Res., 15 (2013) 1-17.

[4] J. Zhao, Z. Wang, J.C. White, B. Xing, Graphene in the aquatic environment: adsorption, dispersion, toxicity and transformation, Environmental science & technology, 48 (2014) 9995-10009.

[5] A.Y. Romanchuk, A.S. Slesarev, S.N. Kalmykov, D.V. Kosynkin, J.M. Tour, Graphene oxide for effective radionuclide removal, PCCP, 15 (2013) 2321-2327.

[6] S. Yu, X. Wang, X. Tan, X. Wang, Sorption of radionuclides from aqueous systems onto graphene oxide-based materials: a review, Inorganic Chemistry Frontiers, (2015).

[7] S.S. Patil, U.U. Shedbalkar, A. Truskewycz, B.A. Chopade, A.S. Ball, Nanoparticles for environmental clean-up: a review of potential risks and emerging solutions, Environmental Technology & Innovation, 5 (2016) 10-21.

[8] C.M. Park, D. Wang, C. Su, Recent Developments in Engineered Nanomaterials for Water Treatment and Environmental Remediation, Handbook of Nanomaterials for Industrial Applications, Elsevier2018, pp. 849-882.

[9] M. Kah, R.S. Kookana, A. Gogos, T.D. Bucheli, A critical evaluation of nanopesticides and nanofertilizers against their conventional analogues, Nature nanotechnology, (2018) 1.

[10] C.O. Dimkpa, P.S. Bindraban, Nanofertilizers: New products for the industry?, J. Agric. Food. Chem., (2017).

[11] H. Ehtesabi, M.M. Ahadian, V. Taghikhani, M.H. Ghazanfari, Enhanced heavy oil recovery in sandstone cores using tio2 nanofluids, Energy & Fuels, 28 (2013) 423-430.

[12] N.H. Pham, D.V. Papavassiliou, Hydrodynamic effects on the aggregation of nanoparticles in porous media, Int. J. Heat Mass Transfer, 121 (2018) 477-487.

[13] P.M. Abraham, S. Barnikol, T. Baumann, M. Kuehn, N.P. Ivleva, G.E. Schaumann, Sorption of silver nanoparticles to environmental and model surfaces, Environmental science & technology, 47 (2013) 5083-5091.

[14] C. Nickel, S. Gabsch, B. Hellack, A. Nogowski, F. Babick, M. Stintz, T.A.J. Kuhlbusch, Mobility of coated and uncoated TiO 2 nanomaterials in soil columns–Applicability of the tests methods of OECD TG 312 and 106 for nanomaterials, Journal of environmental management, 157 (2015) 230-237.

[15] P. Babakhani, J. Bridge, T. Phenrat, R.-a. Doong, K. Whittle, Aggregation and sedimentation of shattered graphene oxide nanoparticles in dynamic environments: a solid-body rotational approach, Environmental Science: Nano, doi: 10.1039/C8EN00443A (2018).

[16] E.M. Hotze, T. Phenrat, G.V. Lowry, Nanoparticle Aggregation: Challenges to Understanding Transport and Reactivity in the Environment, J. Environ. Qual., 39 (2010) 1909–1924.

[17] T. Phenrat, H.J. Kim, F. Fagerlund, T. Illangasekare, R.D. Tilton, G.V. Lowry, Particle size distribution, concentration, and magnetic attraction affect transport of polymer-modified Fe0 nanoparticles in sand columns, Environ. Sci. Technol., 43 (2009) 5079-5085.

[18] T. Phenrat, H.-J. Kim, F. Fagerlund, T. Illangasekare, G.V. Lowry, Empirical correlations to estimate agglomerate size and deposition during injection of a polyelectrolyte-modified Fe0 nanoparticle at high particle concentration in saturated sand, J. Contam. Hydrol., 118 (2010) 152-164.

[19] T. Phenrat, N. Saleh, K. Sirk, R.D. Tilton, G.V. Lowry, Aggregation and sedimentation of aqueous nanoscale zerovalent iron dispersions, Environmental Science & Technology, 41 (2007) 284-290.

[20] T. Phenrat, G.V. Lowry, Nanoscale Zerovalent Iron Particles for Environmental Restoration, Springer2019.

[21] T. Raychoudhury, N. Tufenkji, S. Ghoshal, Aggregation and deposition kinetics of carboxymethyl cellulose-modified zero-valent iron nanoparticles in porous media, Water Res., 46 (2012) 1735-1744.

[22] A.L. Dale, G.V. Lowry, E.A. Casman, Accurate and fast numerical algorithms for tracking particle size distributions during nanoparticle aggregation and dissolution, Environmental Science: Nano, 4 (2017) 89-104.

[23] A.L. Dale, G.V. Lowry, E.A. Casman, Much ado about α: reframing the debate over appropriate fate descriptors in nanoparticle environmental risk modeling, Environmental Science: Nano, (2015).

[24] P. Babakhani, F. Fagerlund, A. Shamsai, G.V. Lowry, T. Phenrat, Modified MODFLOW-based model for simulating the agglomeration and transport of polymer-modified Fe nanoparticles in saturated porous media, Environ Sci Pollut Res, 1-20, doi:10.1007/s11356-015-5193-0, (2018).

[25] P. Babakhani, J. Bridge, R.-a. Doong, T. Phenrat, Continuum-based models and concepts for the transport of nanoparticles in saturated porous media: A state-of-the-science review, Adv. Colloid Interface Sci., 246 (2017) 75-104.

[26] C.D. Tsakiroglou, A. Sikinioti-Lock, K. Terzi, M. Theodoropoulou, A numerical model to simulate the NAPL source zone remediation by injecting zero-valent iron nanoparticles, Chem. Eng. Sci., 192 (2018) 391-413.

[27] L.M. Gilbertson, B.A. Wender, J.B. Zimmerman, M.J. Eckelman, Coordinating modeling and experimental research of engineered nanomaterials to improve life cycle assessment studies, Environmental Science: Nano, 2 (2015) 669-682.

[28] L. Pourzahedi, M. Pandorf, D. Ravikumar, J.B. Zimmerman, T.P. Seager, T.L. Theis, P. Westerhoff, L.M. Gilbertson, G.V. Lowry, Life cycle considerations of nano-enabled agrochemicals: are today's tools up to the task?, Environmental Science: Nano, 5 (2018) 1057-1069.

[29] A.A. Keller, A. Lazareva, Predicted releases of engineered nanomaterials: from global to regional to local, Environmental Science & Technology Letters, 1 (2013) 65-70.

[30] N.C. Mueller, B. Nowack, Exposure modeling of engineered nanoparticles in the environment, Environmental science & technology, 42 (2008) 4447-4453.

[31] D. Mackay, E. Webster, I. Cousins, T. Cahill, K. Foster, T. Gouin, An introduction to multimedia models, CEMC Report, (2001) 30.

[32] B. Nowack, M. Baalousha, N. Bornhöft, Q. Chaudhry, G. Cornelis, J. Cotterill, A. Gondikas, M. Hassellöv, J. Lead, D.M. Mitrano, Progress towards the validation of modeled environmental concentrations of engineered nanomaterials by analytical measurements, Environmental Science: Nano, (2015).

[33] T. Phenrat, F. Fagerlund, T. Illangasekare, G.V. Lowry, R.D. Tilton, Polymer-Modified Fe0 Nanoparticles Target Entrapped NAPL in Two Dimensional Porous Media: Effect of

Particle Concentration, NAPL Saturation, and Injection Strategy, Environmental Science & Technology, 45 (2011) 6102-6109.

[34] F. Fagerlund, T.H. Illangasekare, T. Phenrat, H.J. Kim, G.V. Lowry, PCE dissolution and simultaneous dechlorination by nanoscale zero-valent iron particles in a DNAPL source zone, J. Contam. Hydrol., 131 (2012) 9-28.

[35] H.-J. Kim, T. Phenrat, R.D. Tilton, G.V. Lowry, Effect of kaolinite, silica fines and pH on transport of polymer-modified zero valent iron nano-particles in heterogeneous porous media, J. Colloid Interface Sci., 370 (2012) 1-10.

[36] S.M. Louie, R.D. Tilton, G.V. Lowry, Effects of molecular weight distribution and chemical properties of natural organic matter on gold nanoparticle aggregation, Environmental science & technology, 47 (2013) 4245-4254.

[37] S.M. Louie, R.D. Tilton, G.V. Lowry, Critical review: impacts of macromolecular coatings on critical physicochemical processes controlling environmental fate of nanomaterials, Environmental Science: Nano, 3 (2016) 283-310.

[38] A.L. Dale, E.A. Casman, G.V. Lowry, J.R. Lead, E. Viparelli, M. Baalousha, Modeling Nanomaterial Environmental Fate in Aquatic Systems, Environmental Science & Technology, 49 (2015) 2587-2593.

[39] L. He, L. Xie, D. Wang, W. Li, J.D. Fortner, Q. Li, Y. Duan, Z. Shi, P. Liao, C. Liu, Elucidating the Role of Sulfide on the Stability of Ferrihydrite Colloids under Anoxic Conditions, Environmental science & technology, (2019).

[40] P. Babakhani, R.-a. Doong, J. Bridge, Significance of early and late stages of coupled aggregation and sedimentation in the fate of nanoparticles: measurement and modelling, Environmental science & technology, doi: 10.1021/acs.est.7b05236 (2018).

[41] J.T.K. Quik, D. van De Meent, A.A. Koelmans, Simplifying modeling of nanoparticle aggregation–sedimentation behavior in environmental systems: A theoretical analysis, Water Res., 62 (2014) 193-201.

[42] R. Arvidsson, S. Molander, B.A. Sandén, M. Hassellöv, Challenges in exposure modeling of nanoparticles in aquatic environments, Human and Ecological Risk Assessment, 17 (2011) 245-262.

[43] M.R. Soltanian, A. Sun, Z. Dai, Reactive transport in the complex heterogeneous alluvial aquifer of Fortymile Wash, Nevada, Chemosphere, 179 (2017) 379-386.

[44] M. Therezien, A. Thill, M.R. Wiesner, Importance of heterogeneous aggregation for NP fate in natural and engineered systems, Sci. Total Environ., 485 (2014) 309-318.

[45] A.B. Burd, S.B. Moran, G.A. Jackson, A coupled adsorption–aggregation model of the POC/234Th ratio of marine particles, Deep Sea Research Part I: Oceanographic Research Papers, 47 (2000) 103-120.

[46] M. Elimelech, J. Gregory, X. Jia, Particle deposition and aggregation: measurement, modelling and simulation, Butterworth-Heinemann1998.

[47] I. Szilagyi, T. Szabo, A. Desert, G. Trefalt, T. Oncsik, M. Borkovec, Particle aggregation mechanisms in ionic liquids, PCCP, 16 (2014) 9515-9524.

[48] M. Han, D.F. Lawler, The (relative) insignificance of G in flocculation, Journal (American Water Works Association), (1992) 79-91.

[49] K.W. Lee, Y.J. Lee, D.S. Han, The log-normal size distribution theory for Brownian coagulation in the low Knudsen number regime, J. Colloid Interface Sci., 188 (1997) 486-492.

[50] M. Tourbin, C. Frances, Experimental characterization and population balance modelling of the dense silica suspensions aggregation process, Chem. Eng. Sci., 63 (2008) 5239-5251.

[51] S. Kumar, D. Ramkrishna, On the solution of population balance equations by discretization—I. A fixed pivot technique, Chem. Eng. Sci., 51 (1996) 1311-1332.

[52] J. Kumar, M. Peglow, G. Warnecke, S. Heinrich, An efficient numerical technique for solving population balance equation involving aggregation, breakage, growth and nucleation, Powder Technol., 182 (2008) 81-104.

[53] I. Nopens, D. Beheydt, P.A. Vanrolleghem, Comparison and pitfalls of different discretised solution methods for population balance models: a simulation study, Computers & chemical engineering, 29 (2005) 367-377.

[54] A. Majumder, V. Kariwala, S. Ansumali, A. Rajendran, Lattice Boltzmann method for population balance equations with simultaneous growth, nucleation, aggregation and breakage, Chem. Eng. Sci., 69 (2012) 316-328.

[55] S. Bove, T. Solberg, B.H. Hjertager, A novel algorithm for solving population balance equations: the parallel parent and daughter classes. Derivation, analysis and testing, Chem. Eng. Sci., 60 (2005) 1449-1464.

[56] V. Bedekar, E.D. Morway, C.D. Langevin, M.J. Tonkin, MT3D-USGS version 1: A US Geological Survey release of MT3DMS updated with new and expanded transport capabilities for use with MODFLOW, US Geological Survey, 2016.

[57] T.P. Clement, A Modular Computer Code for Simulating Reactive Multispecies Transport in 3-Dimensional Groundwater Systems, The U.S. Department of Energy, (1997) 1-59.

[58] C. Zheng, MT3D99, A Modular 3D Multispecies Transport Simulator User's Guide, SS Papadopulos & Associates Inc, (2000).

[59] M.J. Hounslow, R.L. Ryall, V.R. Marshall, A discretized population balance for nucleation, growth, and aggregation, AlChE J., 34 (1988) 1821-1832.

[60] J. Lister, D. Smit, M. Hounslow, Adjustable discretized population balance for growth and aggregation, AlChE J., 41 (1995) 591-603.

[61] A.A. Markus, J.R. Parsons, E.W.M. Roex, P. de Voogt, R. Laane, Modeling aggregation and sedimentation of nanoparticles in the aquatic environment, Sci. Total Environ., 506 (2015) 323-329.

[62] M.C. Sterling, J.S. Bonner, A.N.S. Ernest, C.A. Page, R.L. Autenrieth, Application of fractal flocculation and vertical transport model to aquatic sol–sediment systems, Water Res., 39 (2005) 1818-1830.

[63] M. Smoluchowski, Versuch einer mathematischen Theorie der Koagulationskinetik kolloider Lösungen, Zeitschrift fuer Physikalische Chemie. 92., 129-68 (1917).

[64] M. Singh, J. Kumar, A. Bück, A volume conserving discrete formulation of aggregation population balance equations on non-uniform meshes, IFAC-PapersOnLine, 48 (2015) 192-197.

[65] S. Chandrasekhar, Stochastic problems in physics and astronomy, Reviews of modern physics, 15 (1943) 1.

[66] J.R. Hunt, Self-similar particle-size distributions during coagulation: theory and experimental verification, J. Fluid Mech., 122 (1982) 169-185.

[67] J.R. Hunt, Particle aggregate breakup by fluid shear, Estuarine cohesive sediment dynamics, Springer1986, pp. 85-109.

[68] M.B. Seymour, G. Chen, C. Su, Y. Li, Transport and Retention of Colloids in Porous Media: Does Shape Really Matter?, Environmental Science & Technology, 47 (2013) 8391-8398.

[69] B.M. Dolgonosov, Kinetics of sedimentation of a coagulating suspension, Theor. Found. Chem. Eng., 39 (2005) 635-642.

[70] S. Veerapaneni, M.R. Wiesner, Hydrodynamics of fractal aggregates with radially varying permeability, J. Colloid Interface Sci., 177 (1996) 45-57.

[71] P.J. Vikesland, R.L. Rebodos, J.Y. Bottero, J. Rose, A. Masion, Aggregation and sedimentation of magnetite nanoparticle clusters, Environmental Science: Nano, 3 (2016) 567-577.

[72] J.E. Nash, J.V. Sutcliffe, River flow forecasting through conceptual models part I — A discussion of principles, Journal of Hydrology, 10 (1970) 282-290.

[73] Y. Sun, B. Gao, S.A. Bradford, L. Wu, H. Chen, X. Shi, J. Wu, Transport, retention, and size perturbation of graphene oxide in saturated porous media: Effects of input concentration and grain size, Water Res., 68 (2015) 24-33.

[74] L. Liu, B. Gao, L. Wu, Y. Sun, Z. Zhou, Effects of surfactant type and concentration on graphene retention and transport in saturated porous media, Chem. Eng. J., 262 (2015) 1187-1191.

[75] L. Liu, B. Gao, L. Wu, L. Yang, Z. Zhou, H. Wang, Effects of pH and surface metal oxyhydroxides on deposition and transport of carboxyl-functionalized graphene in saturated porous media, J. Nanopart. Res., 15 (2013) 1-8.

[76] B.A. Nordmark, T.M. Przybycien, R.D. Tilton, Comparative coagulation performance study of Moringa oleifera cationic protein fractions with varying water hardness, Journal of Environmental Chemical Engineering, 4 (2016) 4690-4698.

[77] S. Xu, B. Gao, J.E. Saiers, Straining of colloidal particles in saturated porous media, Water Resour. Res., 42 (2006).

[78] W. Um, R.J. Serne, C.F. Brown, K.A. Rod, Uranium (VI) sorption on iron oxides in Hanford Site sediment: Application of a surface complexation model, Appl. Geochem., 23 (2008) 2649-2657.

[79] S.J. Wallace, J. Li, R.L. Nation, B.J. Boyd, Drug release from nanomedicines: selection of appropriate encapsulation and release methodology, Drug delivery and translational research, 2 (2012) 284-292.

[80] M. Holmboe, S. Wold, M. Jonsson, S. Garcia-Garcia, Effects of γ-irradiation on the stability of colloidal Na+-Montmorillonite dispersions, Applied Clay Science, 43 (2009) 86-90.

[81] K. Afshinnia, M. Sikder, B. Cai, M. Baalousha, Effect of nanomaterial and media physicochemical properties on Ag NM aggregation kinetics, J. Colloid Interface Sci., 487 (2017) 192-200.

[82] Y. Jiang, R. Raliya, J.D. Fortner, P. Biswas, Graphene oxides in water: correlating morphology and surface chemistry with aggregation behavior, Environmental science & technology, 50 (2016) 6964-6973.

[83] G. Trefalt, I. Szilagyi, G. Téllez, M. Borkovec, Colloidal Stability in Asymmetric Electrolytes: Modifications of the Schulze–Hardy Rule, Langmuir, 33 (2017) 1695-1704.

[84] P. Rouster, M. Pavlovic, I. Szilagyi, Destabilization of titania nanosheet suspensions by inorganic salts: Hofmeister series and Schulze-Hardy rule, The Journal of Physical Chemistry B, 121 (2017) 6749-6758.

[85] T. Oncsik, G. Trefalt, M. Borkovec, I. Szilagyi, Specific ion effects on particle aggregation induced by monovalent salts within the Hofmeister series, Langmuir, 31 (2015) 3799-3807.

[86] T. Cao, I. Szilagyi, T. Oncsik, M. Borkovec, G. Trefalt, Aggregation of colloidal particles in the presence of multivalent co-ions: The inverse Schulze–Hardy rule, Langmuir, 31 (2015) 6610-6614.

[87] J. Shang, X. Gao, Nanoparticle counting: towards accurate determination of the molar concentration, Chem. Soc. Rev., 43 (2014) 7267-7278.

[88] S.K. Friedlander, Similarity considerations for the particle-size spectrum of a coagulating, sedimenting aerosol, Journal of Meteorology, 17 (1960) 479-483.

[89] J.j. Zhang, X.y. Li, Modeling particle-size distribution dynamics in a flocculation system, AlChE J., 49 (2003) 1870-1882.

[90] D.J. Jeffrey, Quasi-stationary approximations for the size distribution of aerosols, Journal of the Atmospheric Sciences, 38 (1981) 2440-2443.

[91] I. Chowdhury, S.L. Walker, S.E. Mylon, Aggregate morphology of nano-TiO2: role of primary particle size, solution chemistry, and organic matter, Environmental Science: Processes & Impacts, 15 (2013) 275-282.

[92] C. Allain, M. Cloitre, F. Parisse, Settling by cluster deposition in aggregating colloidal suspensions, J. Colloid Interface Sci., 178 (1996) 411-416.

[93] J. Zhang, J. Buffle, Multi-method determination of the fractal dimension of hematite aggregates, Colloids and Surfaces A: Physicochemical and Engineering Aspects, 107 (1996) 175-187.

[94] I. Nopens, P.A. Vanrolleghem, Comparison of discretization methods to solve a population balance model of activated sludge flocculation including aggregation and breakage, Mathematical and Computer Modelling of Dynamical Systems, 12 (2006) 441-454.